

Figure 4.17. Laminate beam structure with one fiber/matrix cell included under torsion loading.

Torsion			
Lamina	E_i/E	$E_{ax,i}/E_{ax}$	$E_{s,i}/E_s$
1	0.353	0.508	0.319
2	0.302	0.021	0.358
3	0.345	0.471	0.323
	$E \times 10^2$ [mJ]	$E_{ax} \times 10^4$ [mJ]	$E_s \times 10^2$ [mJ]
Laminate	7.330	9.671	6.071

Table 4.11. Strain energy distribution in a laminate beam under torsion $F = 1$ N load.

Bending			
Lamina	E_i/E	$E_{ax,i}/E_{ax}$	$E_{s,i}/E_s$
1	0.451	0.499	0.116
2	0.099	0.003	0.772
3	0.450	0.499	0.113
	$E \times 10^1$ [mJ]	$E_{ax} \times 10^1$ [mJ]	$E_s \times 10^2$ [mJ]
Laminate	5.798	5.077	6.833

Table 4.12. Strain energy distribution in a laminate beam under bending $F = 5$ N load.

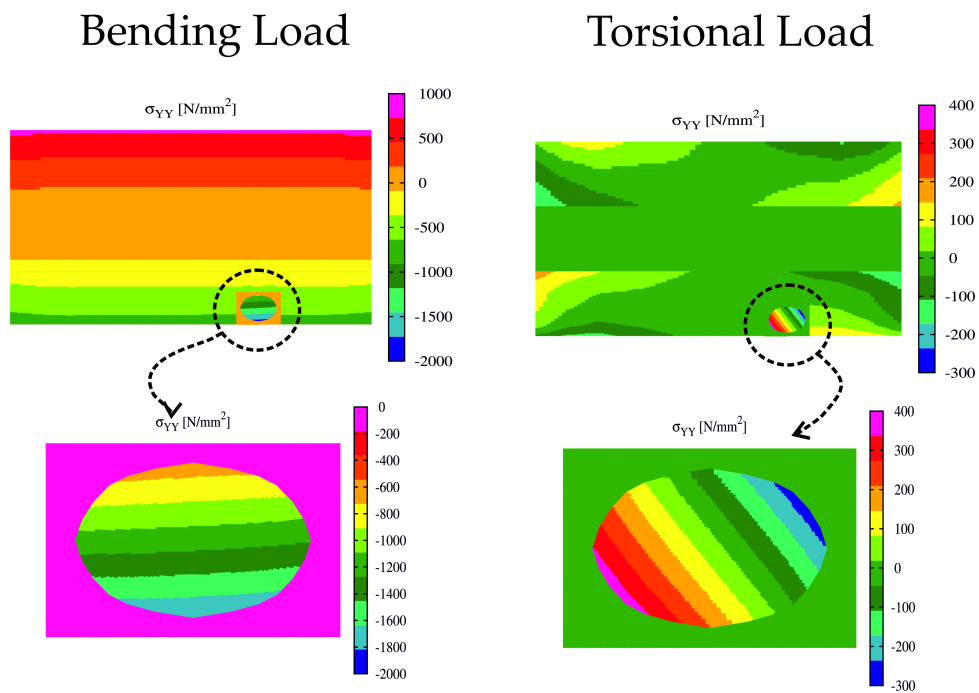


Figure 4.18. Axial stress distribution at the clamped cross section for the laminate beam (one fiber/matrix cell included) under bending and torsion loadings.

the total, axial and shear strain energy of the whole cell for both the loading cases. Also

Torsion			
	E_i/E	$E_{ax,i}/E_{ax}$	$E_{s,i}/E_s$
Matrix	0.875	0.008	0.883
Fiber	0.125	0.992	0.117
	$E \times 10^3$ [mJ]	$E_{ax} \times 10^5$ [mJ]	$E_s \times 10^3$ [mJ]
Cell	2.582	2.977	2.515

Table 4.13. Strain energy distribution in a fiber/matrix cell included in a laminate beam under d torsion $F = 1$ N loads.

Bending			
	E_i/E	$E_{ax,i}/E_{ax}$	$E_{s,i}/E_s$
Matrix	0.026	0.015	0.741
Fiber	0.974	0.985	0.259
	$E \times 10^2$ [mJ]	$E_{ax} \times 10^2$ [mJ]	$E_s \times 10^4$ [mJ]
Cell	2.322	2.289	3.432

Table 4.14. Strain energy distribution in a fiber/matrix cell included in a laminate beam under bending $F = 5$ N loads.

in this case, concerning the bending load, the fiber is the component related to the axial strain energy while the matrix that related to the shear strain energy absorption. When subjected to torsional load the fiber absorbs the 99,2 % of the cell while the 88,3% of the shear energy is absorbed by the matrix. Evaluations of the FI* for the maximum stress criteria are provided for the fiber/matrix cell in Table 4.15. Through the CW approach,

FI* - MS		
	Bending	Torsion
Matrix	0.055	0.147
Fiber	0.266	0.190
Cell	0.182	0.173

Table 4.15. MS Failure index integrated over the fiber,matrix and whole cell subvolumes under bending $F = 5$ N and torsion $F = 1$ N loads.

in a realistic structural configuration failure parameters can be evaluated on components properly refining the model. For the laminate (b), fiber/matrix cells are included in the ply as shown in Figure 4.19. A different mesh of the fiber cross-section is provided as depicted in Figure 4.20 while the mesh of the whole laminate is obtained by means of 184 L9 elements on the cross-section and 4 B3 along the beam axis. The structure is clamped at $y = 0$, a bending loading is applied at the free tip in the center of the second ply, $F = 5$ N. As in the previous case, results are shown in terms of strain energies in Table 4.16 where first, each lamina is chosen as structural subvolume then, each of the eight fibers

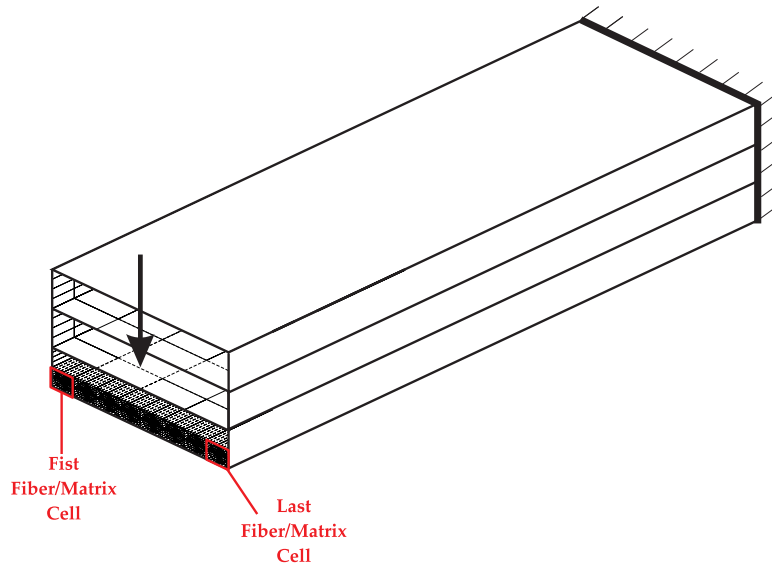


Figure 4.19. Second laminated beam model - laminate (b).

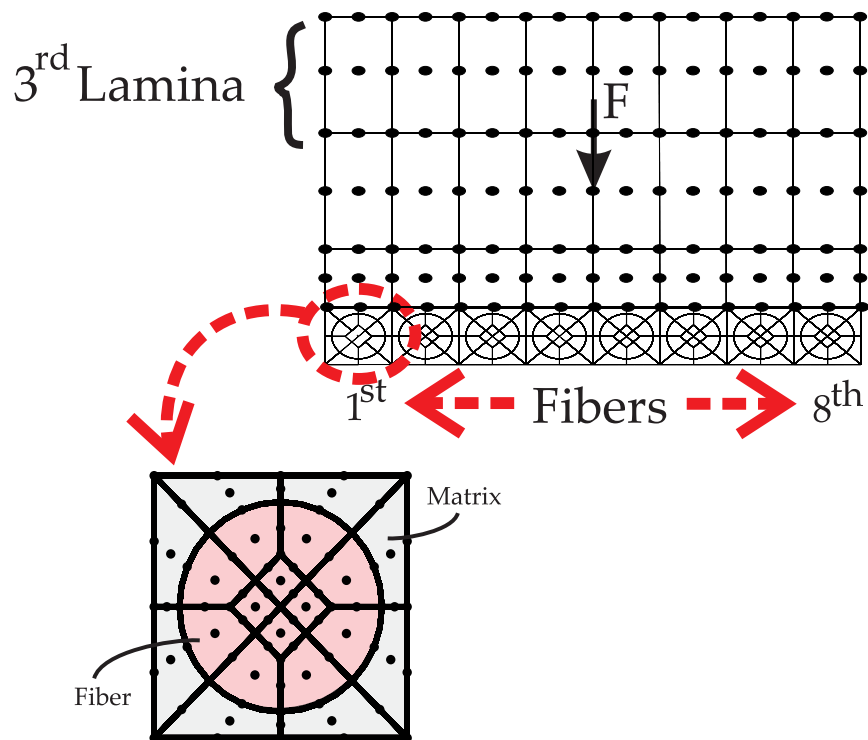


Figure 4.20. Laminate beam structure with eight fiber/matrix cells included under bending loading.

and the related portion of matrix are taken into account. Results are in agreement with

Lamina	E_i/E	$E_{ax,i}/E_{ax}$	$E_{s,i}/E_s$
1	0.462	0.493	0.295
2	0.096	0.003	0.610
3	0.442	0.504	0.095
	$E \times 10^1$ [mJ]	$E_{ax} \times 10^1$ [mJ]	$E_s \times 10^2$ [mJ]
Laminate	5.949	5.052	8.616

Table 4.16. Strain energy distribution in a laminate beam with 8-fiber/matrix cell included under bending $F = 5$ N.

the laminate (a) under bending. For both laminate models, comparison to solid results are provided in Table 4.17. Then, evaluations of the FI* according to the maximum stress

Model	$E \times 10^3$ [mJ]	DOFs
Single Cell		
CW	5.798	17202
Solid	5.946	155403
Eight Cells		
CW	5.949	21033
Solid	6.004	386085

Table 4.17. CW vs Solid. Total energies.

criteria are provided for the fiber/matrix cell in Table 4.18.

FI* - MS			
	Cell	Fiber	Matrix
1	0.293	0.441	0.070
2	0.310	0.469	0.071
3	0.315	0.476	0.074
4	0.312	0.469	0.077
5	0.312	0.469	0.077
6	0.315	0.476	0.074
7	0.310	0.469	0.071
8	0.293	0.441	0.070

Table 4.18. MS Failure index integrated over the fibers, matrix and whole cells subvolumes under bending $F = 5$ N.

Chapter 5

A multiscale approach using the CW cells at the microscale level

A hierarchical multiscale approach for the analysis of fiber-reinforced composite structures is presented in this chapter. A two-scale analysis is proposed; the 1D CUF is used to model the microscale while 3D solid elements are used at the macroscale. The present approach has been implemented in Abaqus environment through a user subroutine UMAT. In section 5.1 the information-passing scheme and the boundary conditions applied at the microscale are introduced. Numerical results are provided in section 5.2 where the present approach is used to perform linear analysis.

5.1 Introduction

In chapter 3 it has been shown how different scales can be simultaneously modeled refining the macroscale model in specific regions. In the CW approach three scales have been considered where the 1D-CUF has been used at each level. A hierarchical multiscale modeling strategy is herein presented. Since scales are hierarchically included in this method, many dimensional levels can be considered by means of different mathematical tools from the molecular dynamics to the continuum mechanics. Nevertheless, the computational cost of the analysis strongly depend on the scales involved in the investigation, a compromise between accuracy and efficiency is then required. Despite the increasing development in computer hardware, the computational effort of these methods is still prohibitive for extensive applications. The reduction of the computational time and cost required to perform failure analysis is still a challenging task. For this reason, the present approach focuses on two scales; a micro- and macro-levels are taken into account by carrying out uncoupled analysis, results are bridged by introducing a proper information-passing scheme. In order to reduce the computational cost of the model, 1D elements have been used at the microscale by means of the CUF while, at the macroscale, 3D elements have been adopted. This approach is based on the micromechanics assumption that in the whole structure a repeating unit cell can be identified. For this reason, entities at the microscale previously addressed as “cells” are herein also referred as Repeating Unit Cells (RUCs).

The macroscale, characterized by the global dimension of the structure to be analyzed, is described as continuum through a homogenized 3D model. The finer scale is characterized by the dimension of the fiber diameters, at this level, the material heterogeneity is introduced modeling the components. The latter scale can be either used to provide the macroscale homogenized stiffness or to model the damage and failure mechanisms within the constituents. If it is used to achieve the former goal, from the knowledge of the material properties at the finer scale the overall behavior of the coarse scale can be predicted to perform linear analysis. If used for the latter, the failure mechanism of the macroscale is obtained as natural evolution of phenomena occurring at the microscale. In the following sections the present multiscale approach is used to perform linear analysis, results of the progressive failure analysis are presented in chapter 6. In the framework of hierarchical multiscale approaches, many different theories have been developed in the last years. A comprehensive overview on two scales analyses is given by Abaudi [57] where the capability in providing the response of elastic, thermoelastic, viscoelastic, and viscoplastic composites has been demonstrated. The initial yield surfaces, strength envelopes, and fatigue failure curves can also be provided through this approaches. Similar methods have previously been developed for aligned short-fiber composites [58]. A review of the Method of Cells (MOC) appeared in [57], and detailed description and application of the method were given in [59]. The MOC was further generalized and reformulated by Paley and Aboudi [40] and [60] and referred as Generalized Method of Cells. Recently, the Integrated Finite Element Method (IFEM) has been introduced for performing progressive failure analysis in fiber reinforced composite structures where both the macro and the microscale are modeled by using 2D and 3D FE. As well as in IFEM, the present work is developed in the framework of the finite element analysis where the macroscale is modeled using the ABAQUS commercial code with 3D elements, while the 1D Carrera Unified Formulation (CUF) is adopted to model the microscale. Since the 1D CUF provides results with accuracy comparable to the solid element modeling, in future works it will be also possible to use it to model both the macroscale and the microscale and have the Integrated CUF (ICUF). In particular, the 1D unified formulation with the LE polynomials, described in section 2.3.2, has been exploited to obtain advanced displacement-based theories. The order of the formulation is a free parameter of the analysis. Using the UF, the stress and strain fields are provided with a significant reduction of DOFs involved. Once a refined description of the stress and strain within the constituent phases is provided, progressive failure analysis can be performed as proposed in section 6.3. Informations obtained by results at the fine scale are passed back to the macroscale assuming that each point can be represented by a unit cell containing fiber and matrix phases as shown in Figure 5.1 where $\langle \sigma \rangle = \int_V \sigma dV$, is the integral of the stress components at the microscale, and dV indicates the volume of the RUC. The far field strain at the integration points can be applied to the cells by means of two different sets of boundary conditions, the linear displacement field and the Periodic Boundary Conditions (PBC). Both set of boundary conditions can be utilized to calculate the homogenized stiffness tensor and update the global state of stress on the cell at the following iteration; an iterative algorithm to solve for the stress field is used. Within similar multiscale approaches progressive failure analysis have been performed using the GMC and the IFEM. A failure criterion at the microscale is used to

determine the failure initiation directly on the components. If such criterion is satisfied, the stiffness of the cell can be progressively reduced. The degraded stiffness is then used to update the global stress on the cell and therefore on the macroscale in which, a loss in the stiffness of the composite is recorded. A detailed description of the failure introduction in the present approach is described in section 6.3 where numerical results are also provided. In the present approach, since the macroscale is modeled in ABAQUS environment, the

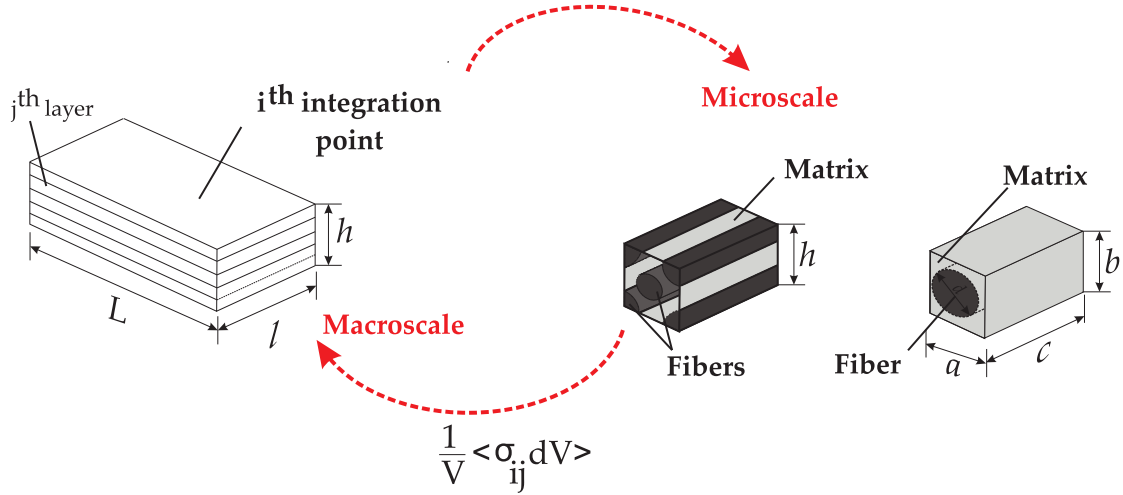


Figure 5.1. Two scales analysis obtained using the 1D CUF at the microscale.

material model has been introduced through a user subroutine (UMAT). The UMAT can be used to define the mechanical constitutive behavior of a material, it will be called at all material calculation points of elements for which the material definition includes a user-defined material behavior. Using the UMAT, the Jacobian matrix of the constitutive model at the microscale, $\frac{\partial \Delta \sigma}{\partial \Delta \epsilon}$, has to be provided where, $\partial \Delta \sigma$ are the stress increments and $\partial \Delta \epsilon$ are the strain increments at each step. The matrix $\frac{\partial \Delta \sigma}{\partial \Delta \epsilon_{[I, J]}}$ defines the change in the i^{th} stress component at the end of the time increment caused by an infinitesimal perturbation of the j^{th} component of the strain increment array. Since no assumptions are made on the stress and strain states, this is a 6×6 matrix. The global value of the stress on the cell to pass back to the macroscale can be evaluated by means of the numerical integral approach described in chapter 4.

5.1.1 Boundary conditions

In a hierarchical multiscale perspective, the correct imposition of boundary conditions at the microscale is of primary importance to solve the problem correctly and passing the informations through the different scales. According to the FE discretization of the cell at the microscale with 1D LE elements, Boundary Conditions (BC) are applied to constrain the stiffness matrix and the loading vector of the linear system to be solved described in chapter 2.

Linear displacement field

Assume a cell of dimensions l_1, l_2, l_3 respectively in x-,y-,z-directions as shown in Figure 5.2. A linear displacement field can be imposed on the cell as in Equation 5.3 where 9

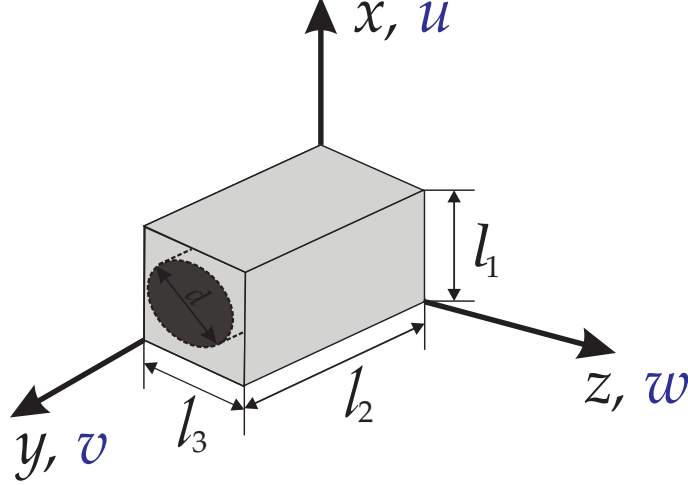


Figure 5.2. Microscale dimensions and reference system for a generic RUC.

coefficients $a_{11}, a_{12}, a_{13}, a_{21}, a_{22}, a_{23}, a_{31}, a_{32}, a_{33}$. have to be determined.

$$\begin{cases} u(x,y,z) = a_{11}x + a_{12}y + a_{13}z \\ v(x,y,z) = a_{21}x + a_{22}y + a_{23}z \\ w(x,y,z) = a_{31}x + a_{32}y + a_{33}z \end{cases} \quad (5.1)$$

Since the macroscale far field strain is known and the geometrical relations are given:

$$\begin{aligned} \varepsilon_{xx} = \frac{\partial u}{\partial x} = a_{11}; \quad \varepsilon_{yy} = \frac{\partial v}{\partial y} = a_{22}; \quad \gamma_{xy} = \frac{\partial u}{\partial y} + \frac{\partial v}{\partial x} = a_{12} \\ \varepsilon_{zz} = \frac{\partial w}{\partial z} = a_{33}; \quad \gamma_{xz} = \frac{\partial u}{\partial z} + \frac{\partial w}{\partial x} = a_{13} \quad \gamma_{yz} = \frac{\partial v}{\partial z} + \frac{\partial w}{\partial y} = a_{23} \end{aligned} \quad (5.2)$$

we can impose:

$$\omega_z = \frac{\partial v}{\partial x} - \frac{\partial u}{\partial y} = 0; \quad \omega_x = \frac{\partial v}{\partial z} + \frac{\partial w}{\partial y} = 0 \quad \omega_y = \frac{\partial u}{\partial z} + \frac{\partial w}{\partial x} = 0 \quad (5.3)$$

and determine the 9 coefficients. The BC are enforced by means of lagrange multipliers, the stiffness matrix is then modified as reported in Equation 5.4 and the force vector as shown in Equation 5.5.

$$[K] \rightarrow \begin{bmatrix} K_{ii} & B^T \\ B & 0 \end{bmatrix} \quad (5.4)$$

where B is the identity matrix with dimension $N_{LM} \times N_{LM}$, where N_{LM} is the number of Lagrange Multipliers $\lambda_i, i = 1, \dots, N_{LM}$.

$$[F] \rightarrow \begin{bmatrix} F_i \\ \lambda_j \end{bmatrix} \quad (5.5)$$

The total number of degree of freedoms, DOFs', is $DOFs' = DOF + N_{LM}$.

$$\begin{aligned}
 a_{11} &= \varepsilon_{xx} \\
 a_{12} &= \frac{\gamma_{xy}}{2} \\
 a_{13} &= \frac{\gamma_{xz}}{2} \\
 a_{21} &= \frac{\gamma_{xy}}{2} \\
 a_{22} &= \varepsilon_{yy} \\
 a_{23} &= \frac{\gamma_{yz}}{2} \\
 a_{31} &= \frac{\gamma_{xz}}{2} \\
 a_{32} &= \frac{\gamma_{yz}}{2} \\
 a_{33} &= \varepsilon_{zz}
 \end{aligned} \tag{5.6}$$

Periodic boundary conditions

Periodic Boundary Conditions (PBC) can also be applied to model the periodicity of the microscale. When the periodicity is enforced it is assumed that the displacement field at opposite faces of the cell is the same. That is, each cell could be placed close to each other as it is since the deformed shapes match. Displacement u, v, w of the boundary nodes of each cell are constrained as shown in Equations 5.7, 5.8 and 5.9 respectively for sides 1, 2 and 3. Sides refer to the cell faces as shown in Figure 5.3 where l_1, l_2, l_3 are the characteristic lengths of the cell respectively in x-, y- and z-directions.

$$Side\ 1 : \begin{cases} u(l_1, y, z) - u(0, y, z) = \varepsilon_{11} l_1 \\ v(l_1, y, z) - v(0, y, z) = 2 \varepsilon_{12} l_1 \\ w(l_1, y, z) - w(0, y, z) = 2 \varepsilon_{13} l_1 \end{cases} \tag{5.7}$$

$$Side\ 2 : \begin{cases} u(x, l_2, z) - u(x, 0, z) = 2 \varepsilon_{21} l_2 \\ v(x, l_2, z) - v(x, 0, z) = \varepsilon_{22} l_2 \\ w(x, l_2, z) - w(x, 0, z) = 2 \varepsilon_{23} l_2 \end{cases} \tag{5.8}$$

$$Side\ 3 : \begin{cases} u(x, y, l_3) - u(x, y, 0) = 2 \varepsilon_{31} l_3 \\ v(x, y, l_3) - v(x, y, 0) = 2 \varepsilon_{32} l_3 \\ w(x, y, l_3) - w(x, y, 0) = \varepsilon_{33} l_3 \end{cases} \tag{5.9}$$

Since the LE formulation is exploited, PBC are directly enforced on the structural nodes of the RUC. A basic example is presented as follows where a square homogeneous RUC is taken into account as shown in Figure 5.4. The 1D LE mesh is obtained using 1 L9 element on the cross-section while 1 B3 element is used along the beam axis. Considering the equivalent 3D volume given by the virtual extrusion of the cross-section geometry along the beam axis there are 27 structural nodes of which. the nodes $(1, \dots, 9)'$ belong to the first beam element node, the nodes $(1, \dots, 9)''$ and $(1, \dots, 9)'''$ respectively to the second and the third element nodes. PBC of side 1 is applied on nodes $i: 5', 6', 7'$ and respectively

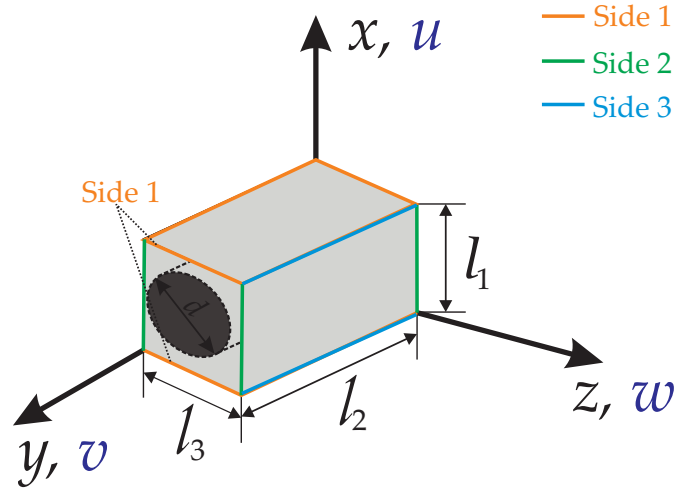


Figure 5.3. PBC side notations.

j: 3', 2', 1', Side 2 on nodes i: 3', 4', 5' and j: 1', 8', 7', while Side 3 on nodes i: 1''', ..., 9''' and j: 1', ..., 9'. The displacement field for a single fiber/matrix RUC is shown in Figure 5.5 where respectively the u_x (u), u_y (v) and u_z (w) components are obtained applying the strain $\varepsilon = 1 \times 10^{-6}$. The PBC are implemented by means of the penalty approach in the

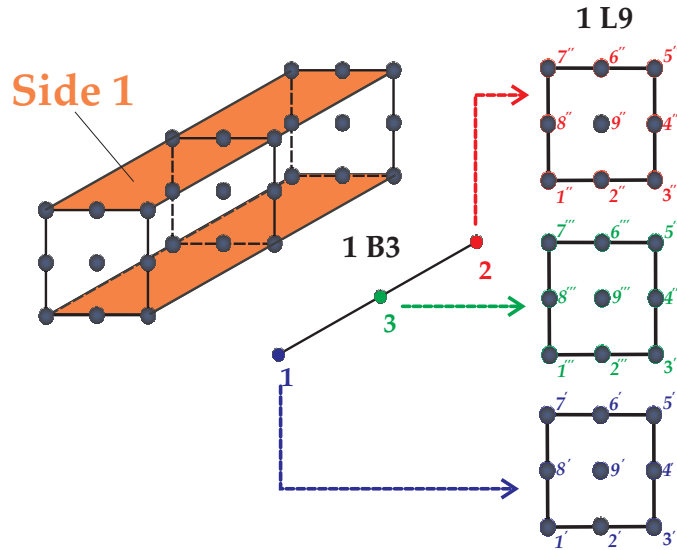


Figure 5.4. PBC applied on a square homogeneous RUC, 1 L9 (cross-section) and 1 B3 (beam axis) elements.

FEM framework. PBC reported in Equations 5.7, 5.8 and 5.9 are multipoint constrain boundary conditions:

$$\beta_{1i}u_i(x,y,z) + \beta_{2j}u_j(x,y,z) = \beta_{0i} \quad i,j = 1,\dots,N \quad (5.10)$$

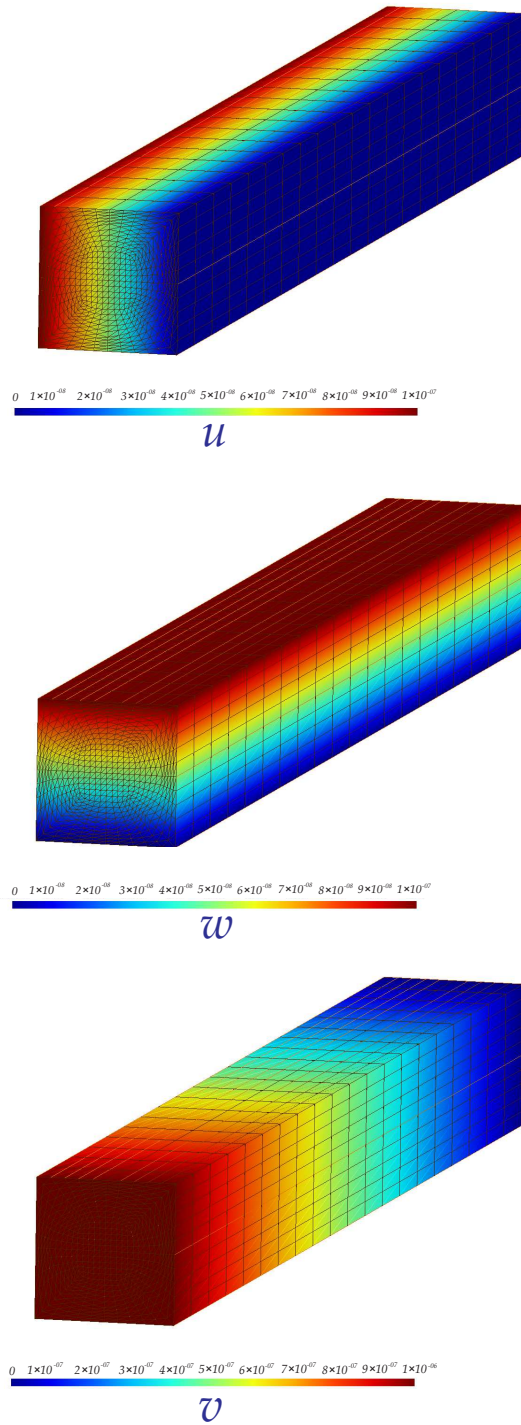


Figure 5.5. Displacement field (u,v,w) on the single fiber/matrix cell due to the PBC.

where $\beta_{1i} = 1$ $\beta_{2j} = -1$ and N is the number of constrains. Introducing this set of constrains, the stiffness matrix and the force vector are shown in Equations 5.11 and 5.12 where C is a penalty value properly chosen depending on the maximum value of the actual stiffness matrix.

$$[K] \rightarrow \begin{bmatrix} K_{ii} + C\beta_{1i}^2 & K_{ij} + C\beta_{1i}\beta_{2j} \\ K_{ji} + C\beta_{1i}\beta_{2j} & K_{jj} + C\beta_{2j}^2 \end{bmatrix} \quad (5.11)$$

$$[F] \rightarrow \begin{bmatrix} F_i + C\beta_{0i}\beta_{1i} \\ F_j + C\beta_{0i}\beta_{2j} \end{bmatrix} \quad (5.12)$$

5.2 Numerical Results

Numerical results for two different case studies are herein presented. A noched laminate is analyzed in section 5.2.1 while an open hole plate is taken into account in section 5.2.2. Both the notched and the open hole plates are subjected to uniaxial tension. The macroscale is modeled in Abaqus environment while for the microscale cells are described through the 1D CUF with LE polynomials. Results are compared with an equivalent homogenized model.

5.2.1 Notched laminate subjected to uniaxial tension

A one layer notched laminate subjected to uniaxial tension is herein analyzed. The laminate geometry is shown in Figure 5.7; dimensions are reported in Table 5.1. The macroscale mesh is obtained as shown in Figure 5.9 by means of solid 8 nodes elements (C3D8). Different unit cells are taken into account at the microscale level. First, a single Fiber/Matrix cell depicted in Figure 5.6 a is taken into account. Then a Hexagonally Packed cell is considered as shown in Figure 5.6 b. In the first case, the cell is square with $l_1 = l_3 = 0.1 \text{ mm}$, $l_2/l_1 = 10$. The fiber ν_f and matrix ν_m volume fractions are $\nu_f = 50.3\%$, $\nu_m = 49.7\%$. The hexagonally packed cell dimensions are $l_1 = 0.1 \text{ mm}$, $l_3 = 0.13$ with $l_2/l_1 = 10$,

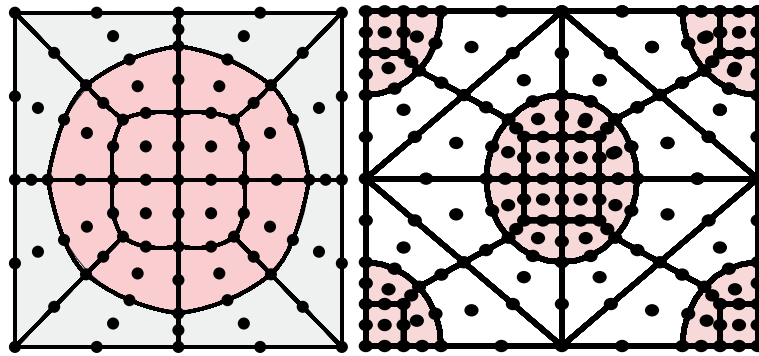


Figure 5.6. Single Fiber/Matrix RUC (20 L9) and Hexagonally Packed cell (40 L9) meshes.

the fiber and matrix volume fractions are $\nu_f = 39 \%$, $\nu_m = 61 \%$. Material properties are respectively $E_f = 250634 \text{ MPa}$, $\nu_f = 0.2456$ for the fibers and $E_m = 3252 \text{ MPa}$,

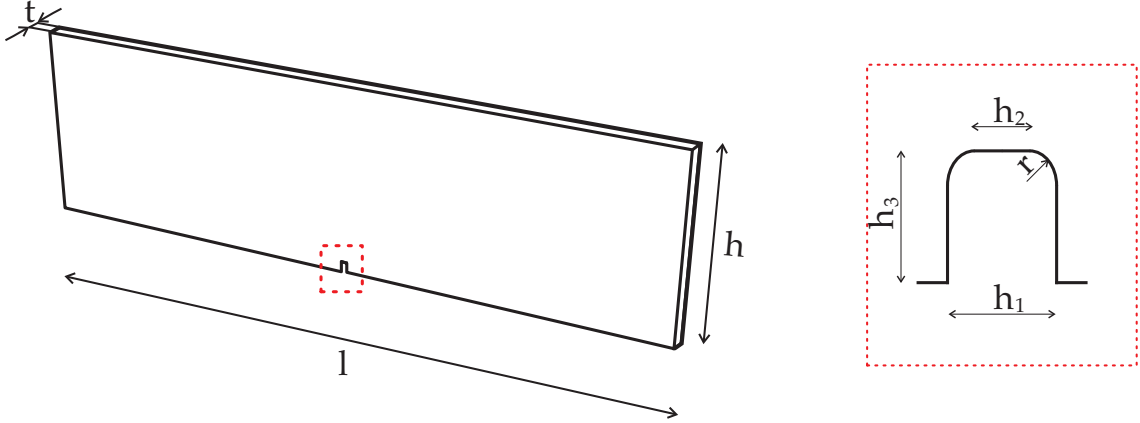


Figure 5.7. Notched one layer laminate geometry.

	[mm]
l	21.65
h	6.35
t	0.13
h_1	0.22
h_2	0.12
h_3	0.38
h_4	0.05

Table 5.1. Notched laminate dimensions.

$\nu_m = 0.355$ for the matrix portions. The laminate is clamped at one end while displacement $u = 0.01$ mm is applied to the opposite side of the structure as shown in Figure 5.8. PBC are applied at the microscale. The Abaqus solid mesh is provided in Figure 5.9. A

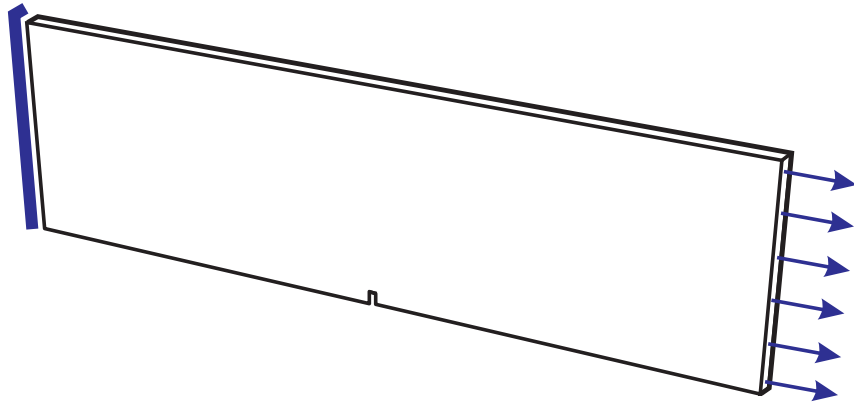


Figure 5.8. Macroscale boundary conditions for the notched laminate model.

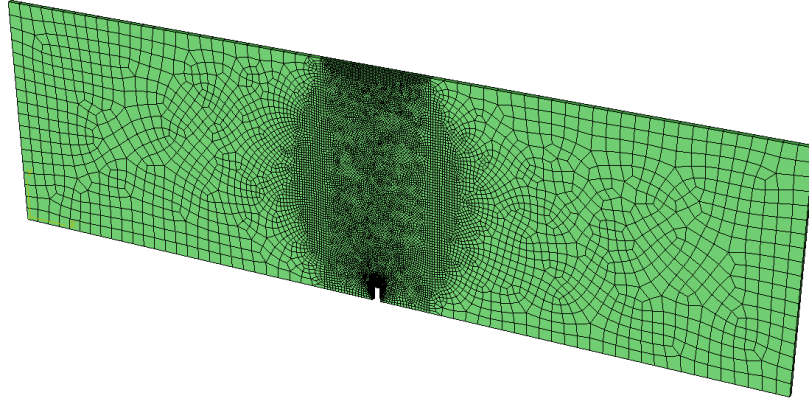


Figure 5.9. Abaqus C3D8 solid mesh.

linear analysis is performed in multiscale perspective and compared with an homogenized model. At each integration point of the solid elements the 1D CUF cell is called to solve the boundary problem and compute the average value of the stress to pass back to the macroscale. The Newton's algorithm is used to solve the linear system in Abaqus. The constitutive equations are implemented through a UMAT subroutine where the Incremental Jacobian matrix has to be defined. For the present case study using the fiber/matrix cell the Jacobian matrix is reported in Equation 5.13.

$$\frac{\partial \Delta \sigma}{\partial \Delta \varepsilon} = \begin{bmatrix} 127073 & 5328 & 5335 & 0 & 0 & 0 \\ 5328 & 13370 & 4732 & 0 & 0 & 0 \\ 5335 & 4732 & 1339 & 0 & 0 & 0 \\ 0 & 0 & 0 & 6903 & 0 & 0 \\ 0 & 0 & 0 & 0 & 6916 & 0 \\ 0 & 0 & 0 & 0 & 0 & 5075 \end{bmatrix} \quad (5.13)$$

The correspondent values for the macroscale elastic properties are:

$$\begin{aligned} E_{11} &= 123935 \text{ [MPa]} \\ E_{22} &= 11603 \text{ [MPa]} \\ E_{33} &= 11626 \text{ [MPa]} \\ \nu_{12} = \nu_{13} &= 0.294 \\ \nu_{32} &= 0.343 \\ G_{12} &= 6904 \text{ [MPa]} \\ G_{23} &= 5075 \text{ [MPa]} \\ G_{13} &= 6916 \text{ [MPa]} \end{aligned} \quad (5.14)$$

The Jacobian Matrix for the hexagonally packed cell is shown in Equation 5.15.

$$\frac{\partial \Delta \sigma}{\partial \Delta \varepsilon} = \begin{bmatrix} 80475 & 4032 & 4015 & 0 & 0 & 0 \\ 4032 & 8318 & 4455 & 0 & 0 & 0 \\ 4015 & 4455 & 8249 & 0 & 0 & 0 \\ 0 & 0 & 0 & 4473 & 0 & 0 \\ 0 & 0 & 0 & 0 & 4374 & 0 \\ 0 & 0 & 0 & 0 & 0 & 4562 \end{bmatrix} \quad (5.15)$$

The correspondent values for the macroscale elastic properties for the hexagonal packed cell are:

$$\begin{aligned} E_{11} &= 77933 \text{ [MPa]} \\ E_{22} &= 5868 \text{ [MPa]} \\ E_{33} &= 5819 \text{ [MPa]} \\ \nu_{32} = \nu_{13} &= 0.3165 \\ \nu_{12} &= 0.3152 \\ G_{12} &= 4473 \text{ [MPa]} \\ G_{23} &= 4374 \text{ [MPa]} \\ G_{13} &= 4562 \text{ [MPa]} \end{aligned}$$

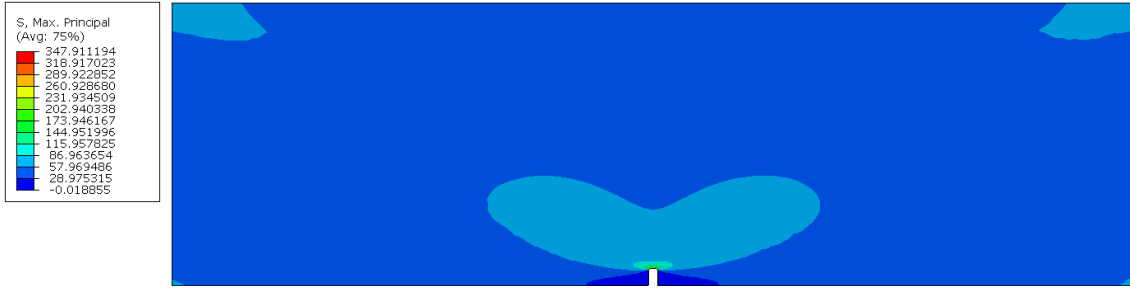


Figure 5.10. Maximum principal stress distribution: multiscale analysis applied at the notched laminate case study.

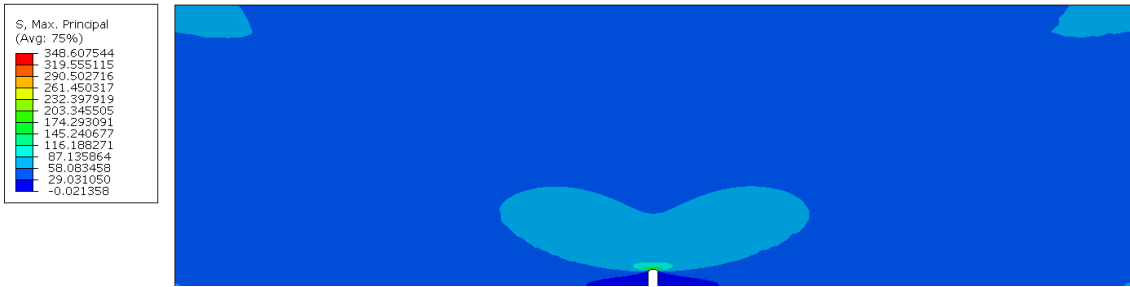


Figure 5.11. Maximum principal stress distribution obtained through the homogenized model for the notched laminate case.

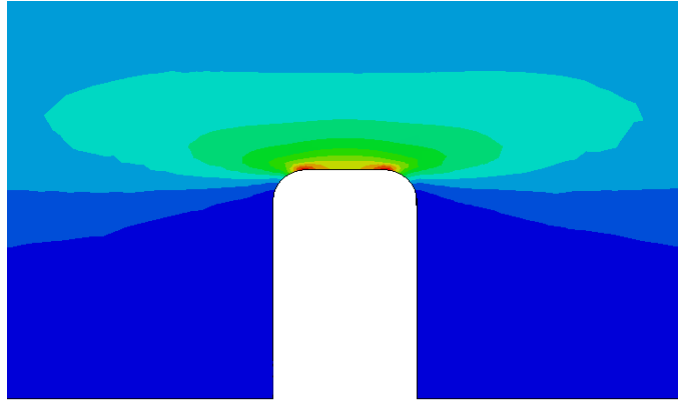


Figure 5.12. Maximum principal stress distribution in the notched area: multiscale analysis.

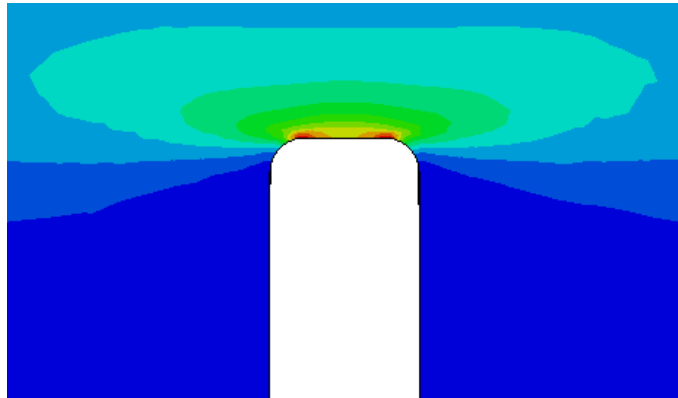


Figure 5.13. Maximum principal stress distribution in the notched area: homogenized model.

5.2.2 Open hole plate subjected to uniaxial tension

Numerical results for an open hole plate are herein presented. The geometry of the structure is shown in Figure 5.2.2 where the length, l , is equal to 150 mm, the width, w , is equal to 100 mm and the thickness of the plate, t , is 5 mm. The characteristic dimension $w/D = 5$ with d diameter of the open hole. The same material properties of the notched laminate analyzed in 5.2.1 have been considered. In Figure 5.2.2, 5.2.2 and 5.2.2 results are shown in terms of stress distribution between the multiscale approach and the homogenized model.

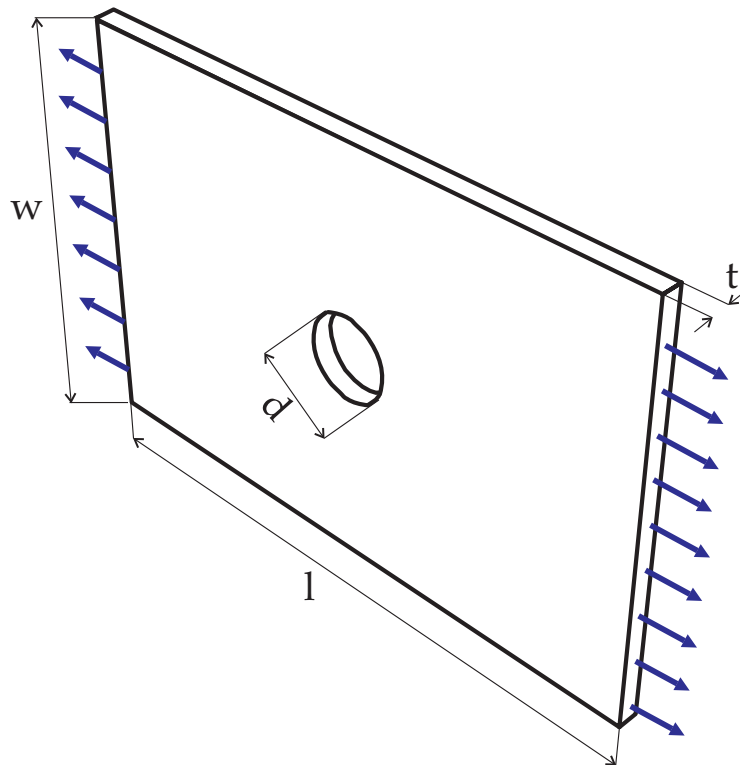


Figure 5.14. Open hole plate under tension.

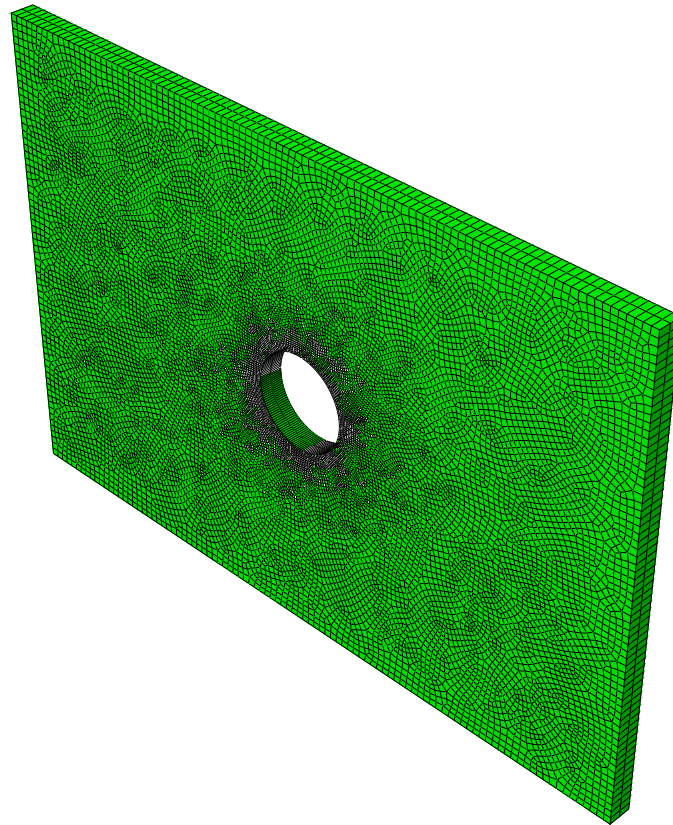
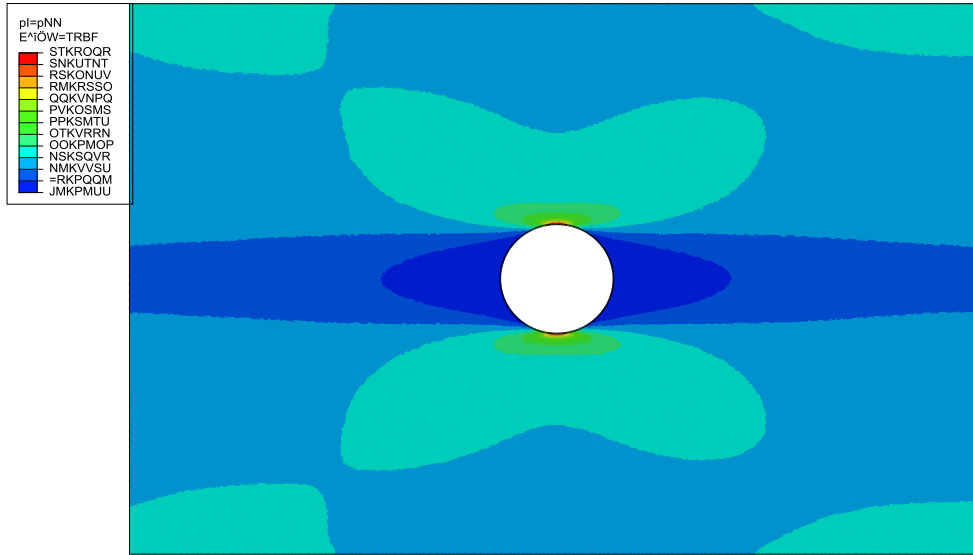
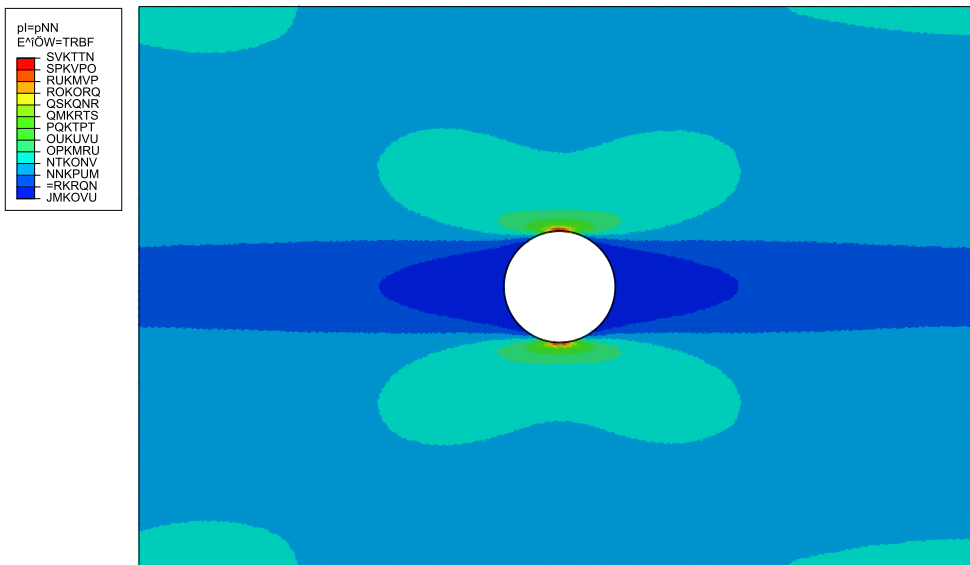


Figure 5.15. Open Hole laminate solid macroscale mesh.

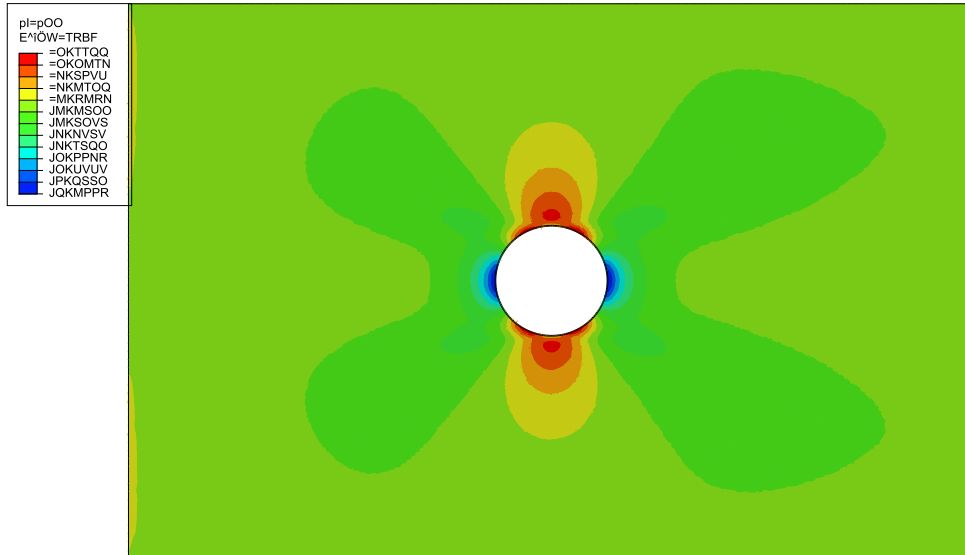


(a)

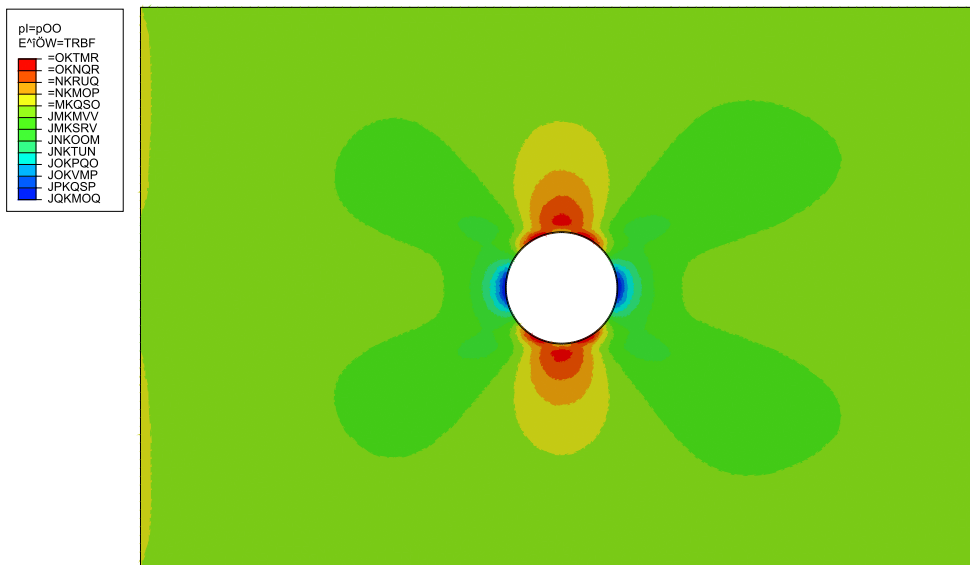


(b)

Figure 5.16. σ_{11} obtained through a multiscale analysis with the single fiber/matrix cell at the microscale (a) and through the homogenized model (b).

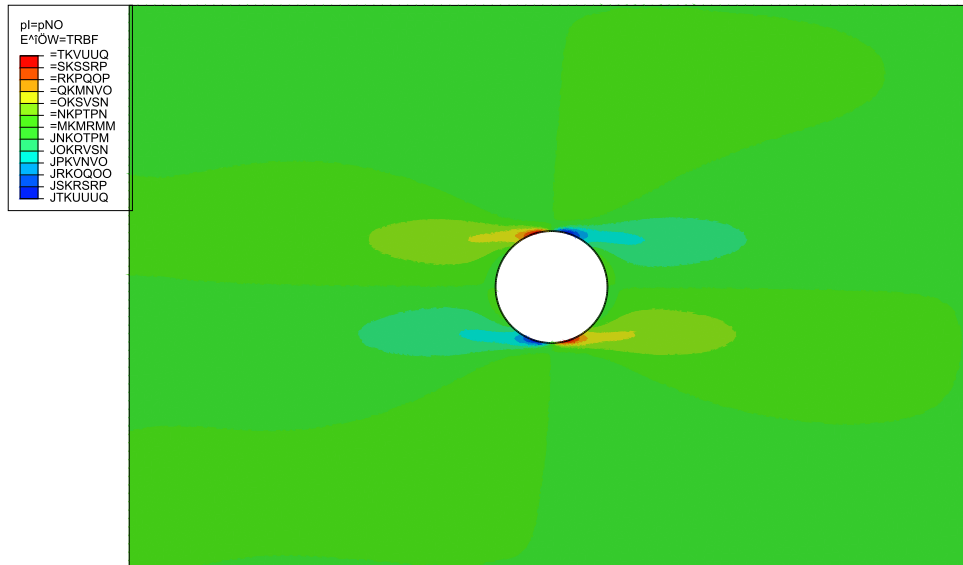


(a)

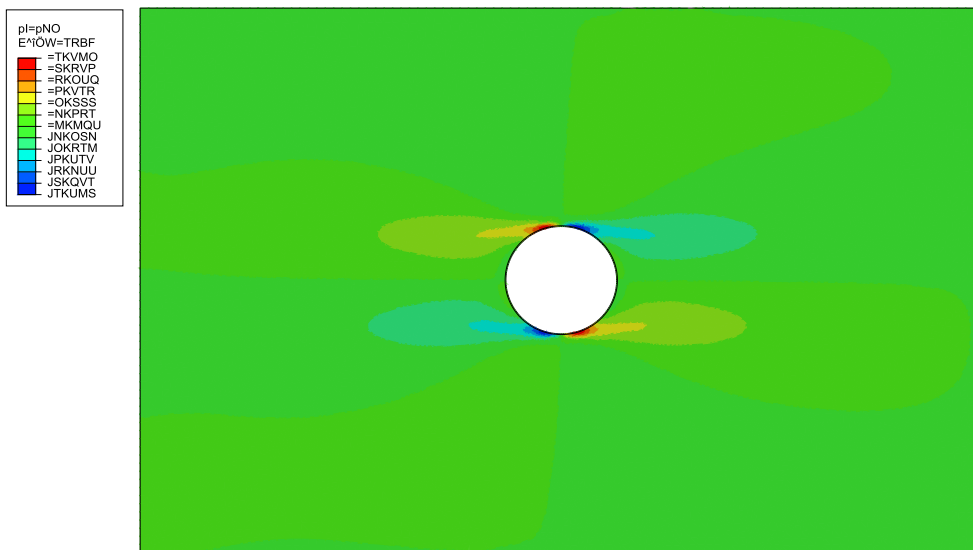


(b)

Figure 5.17. σ_{22} obtained through a multiscale analysis with the single fiber/matrix cell at the microscale (a) and through the homogenized model (b).



(a)



(b)

Figure 5.18. σ_{12} obtained through a multiscale analysis with the single fiber/matrix cell at the microscale(a) and through the homogenized model (b).